Supplementary Information

Switchable Reinforced Streptavidin

Leonard C. Schendel,[‡a] Steffen M. Sedlak,[‡a] and Hermann E. Gaub[*a]

[a]Lehrstuhl für Angewandte Physik and Center for NanoScience, Ludwig-Maximilians-Universität München, Amalienstr. 54, 80799 Munich, Germany

Table of contents

I. Sequences of the Protein Constructs

Functional SA subunit with N-terminal glycines (purple), two mutations to cysteines (T18C,A33C; orange) and C-terminal polyhistidine tag (green):

M**GG**S**EAGI**C**GTWYNQLGSTFIVT**C**GADGALTGTYESAVGNAESRYVLTGRYDSAPATDGSGTALGWTVA**
WKNNYRNAHSATTWSGQYVGGAEARINTQWLLTSGTTEANAWKSTLVGHDTFTKVKPSAASLE**HHHH**
HH

Non-functional SA subunit with the three mutations N23A, S27D, S45A (red):

M**EAGITGTWY**A**QLG**D**TFIVTAGADGALTGTYE**A**AVGNAESRYVLTGRYDSAPATDGSGTALGWTVAWK**
NNYRNAHSATTWSGQYVGGAEARINTQWLLTSGTTEANAWKSTLVGHDTFTKVKPSAAS

ddFLN4 construct with N-terminal ybbR-tag (blue) and polyhistidine tag (green) as well as C-terminal Sortase motif (magenta). The internal cysteine 18 is mutated to serine (red):

M**DSLEFIASKLAHHHHHH**GS**ADPEKSYAEGPGLDGGE**S**FQPSKFKIHAVDPDGVHRTDGGDGFVVTIEGP**
APVDPVMVDNGDGTYDVEFEPKEAGDYVINLTLDGDNVNGFPKTVTVKPAPGSGSGSGS**LPETGG**

ddFLN4 construct with N-terminal Fgβ-peptide (cyan), C-terminal polyhistidine tag (green) and ybbR-tag (blue):

MAT**NEEGFFSARGHRPLD**GSGSGSGSAGTGSG**ADPEKSYAEGPGLDGGE**S**FQPSKFKIHAVDPDGVHRT**
DGGDGFVVTIEGPAPVDPVMVDNGDGTYDVEFEPKEAGDYVINLTLDGDNVNGFPKTVTVKPAPSG**HH**
HHHHGS**DSLEFIASKLA**LPETGG

II. Site-directed Mutagenesis

All mutations were introduced following the Quik Change™ (Stratagene, La Jolla, USA) PCR procedure.

DNA-primer sequences:

Introduce an N-terminal glycine:
Fw: GAAGGAGATATACATATGGGCGGCTCCGAAGCG
Rv: CGCTTCGGAGCCGCCCATATGTATATCTCCTTC

T18C:
Fw: GGCTCCGAAGCGGGGATTTGCGGCACGTGG
Rv: CCACGTGCCGCAAATCCCCGCTTCGGAGCC

A33C:
Fw: GGGTTCCACCTTTATCGTGACTTGTGGGGCAGATGG
Rv: CCATCTGCCCCACAAGTCACGATAAAGGTGGAACCC

Howarth *et al.*[1] deposited pET21a plasmids containing dead/alive SA subunits on addgene.

III. Sodium Dodecyl Sulfate-Polyacrylamide Gel Electrophoresis

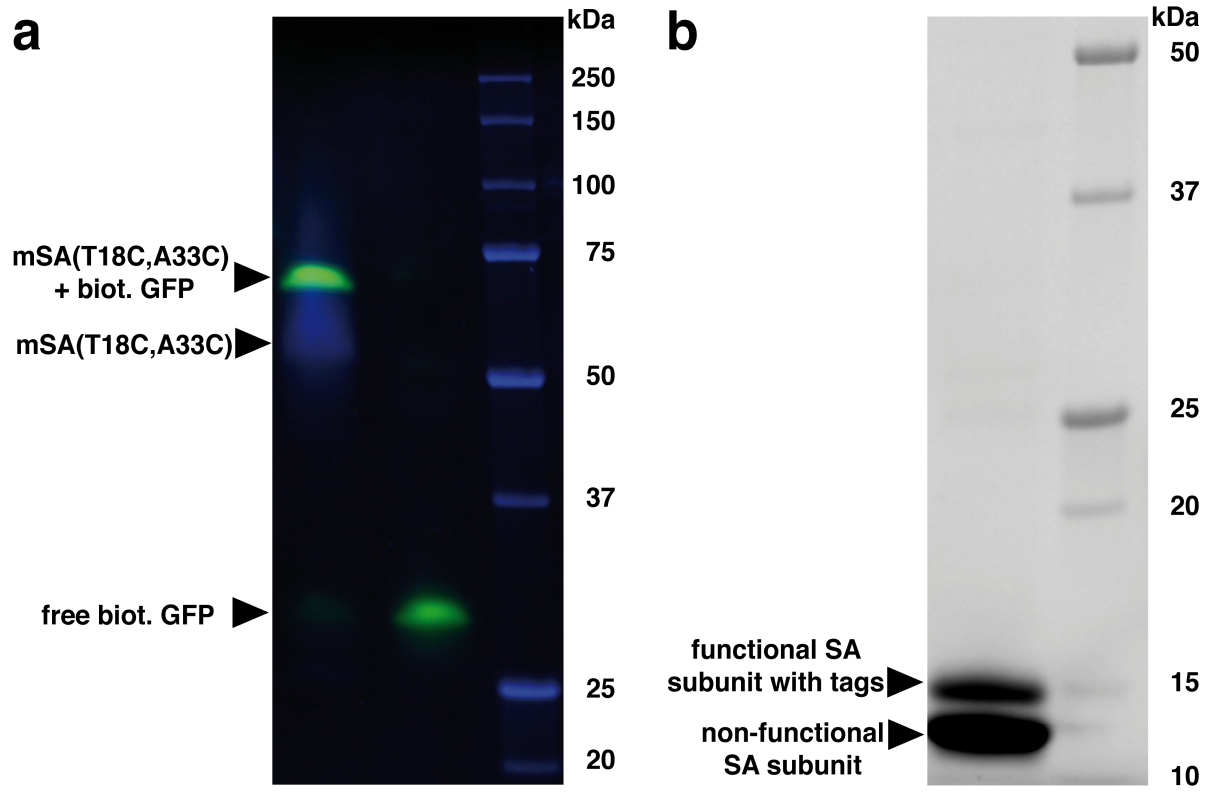

Supplementary Figure S1. SDS-PAGE for protein characterization. (a) mSA construct incubated with biotinylated GFP (left lane), a control with free biotinylated GFP (middle lane), and molecular weight standards (right lane) were run on gel and imaged in the UV channel (blue) and the 488 nm-channel (green). (b) mSA disintegrated into its subunits (left lane) and molecular weight standards (right lane) are shown. The two bands in the left lane correspond to the functional subunit with the additional polyhistidine tag and the non-functional subunits.

Biotinylated GFP was used to check mSA's functionality. An Any kD Mini-PROTEAN TGX Stain-Free Protein Gel (Bio-Rad Laboratories GmbH, Feldkirchen, Germany) was run without prior sample heating to maintain proteins' structure and to keep biotinylated GFP bound to mSA. The gel was imaged on a ChemiDoc MP Imaging System (Bio-Rad Laboratories GmbH, Feldkirchen, Germany) in the UV channel and the 488 nm-channel. mSA construct was incubated with biotinylated GFP before transferring into SDS loading buffer (50 mM TRIS, pH 8.0, 2.5% SDS, 5% glycerol, 0.005% bromphenol blue, 2.5% β-mercaptoethanol). In addition, a control with free biotinylated GFP and molecular weight standards (Precision Plus Protein Standards, Bio-Rad Laboratories GmbH, Feldkirchen, Germany) were run. The observed molecular weights agree well with what was calculated from the amino acid sequence (GFP: 26.9 kDa, mSA: 54.5 kDa). Only the complex of biotinylated GFP and mSA run slightly faster. The gel confirms the monovalency of the mSA construct.

When mSA is heated to 95°C for 5 min prior to gel loading, it disintegrates into its subunits. For the functional subunit with the additional polyhistidine tag the molecular weight (calculated from the amino acid sequence) reads 14.5 kDa, while for the non-functional subunit the molecular weight is only 13.2 kDa. By gel electrophoresis, these weights could be confirmed (Supplementary Fig. S1b). To also check the 3:1-composition of mSA, the lane was quantitatively analysed (Supplementary Fig. S2).

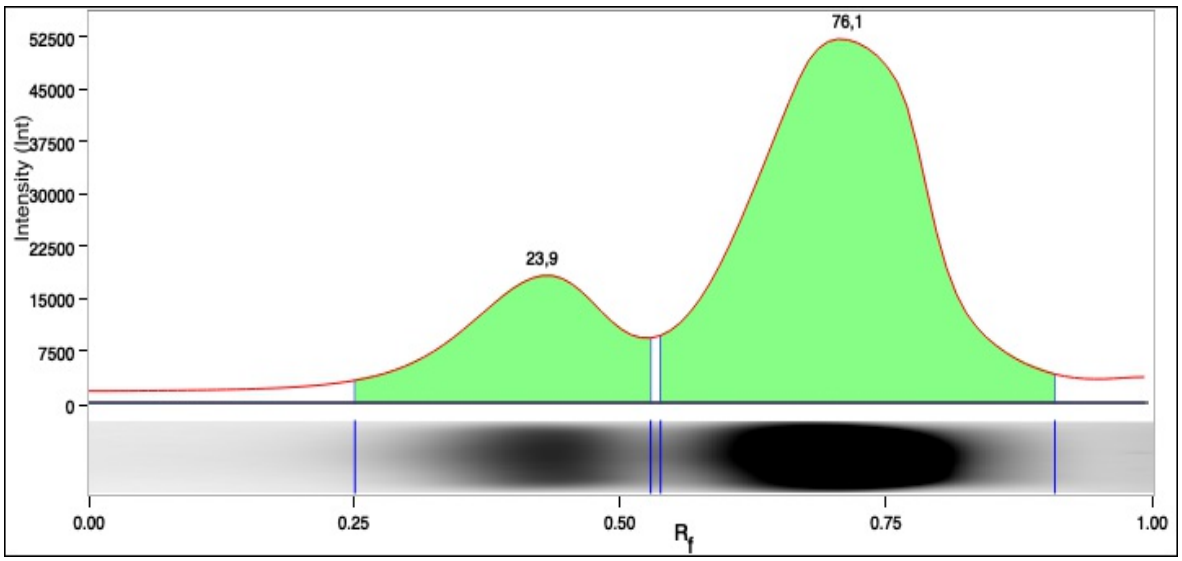

Supplementary Figure S2. Lane profile for heated mSA, decomposed into its subunits. The bands observed in the left lane in Figure S1 were quantitatively analysed using the Image Lab Software (Bio-Rad, Hercules, USA). About one fourth of the subunits are observed in the band corresponding to the functional subunits, the other three fourth in the band corresponding to the non-functional subunit. With SDS PAGE, it was thus possible to quantitatively confirm the composition of mSA – it is comprised of one functional and three non-functional subunits.

IV. Fluorescence Anisotropy

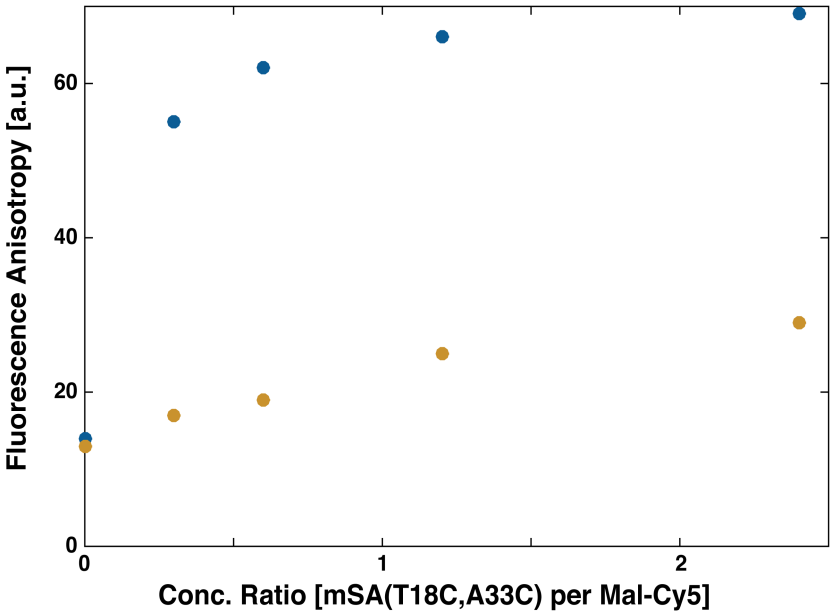

Supplementary Figure S3. Fluorescence Anisotropy of a Cy5-maleimide dye with different concentrations of mSA(T18C,A33C) added in reducing (with TCEP, blue) and oxidizing (without TCEP, yellow) environments.

To detect the disulfide bridge by other means than SMFS, we performed fluorescence anisotropy measurements using a Cy5-maleimide dye. 0.2 µM Cy5-maleimide dye were added to 0, 0.3, 0.6, 1.2 and 2.4 µM mSA(T18C,A33C). Fluorescence anisotropy of the Cy5-maleimide dye was measured on a Tecan Infinite M1000 Pro (Tecan Group AG, Männedorf, Switzerland) in well-plates with and without 1 mM BondBreaker TCEP Solution in the measurement buffer (PBS). In the absence of mSA(T18C,A33C), the fluorescence anisotropy of freely diffusing Cy5-maleimide is comparable for both samples (with and without TCEP). For higher concentrations of mSA(T18C,A33C), we found the fluorescence anisotropy of the Cy5-maleimide dye to increase – probably because the dye is reacting with the much larger mSA(T18C,A33C) and thus its rotational movement is slowed down. In the presence of TCEP (blue data in Supplementary Fig. S3), the disulfide bridge in mSA(T18C,A33C) is reduced and the cysteines' thiols are accessible and can react with the Cy5-maleimide dye. If there is no TCEP in the measurement buffer, the thiols have mainly formed a disulfide bridge. Reaction of Cy5-maleimide to primary amines is possible but not favored at pH 7.4.

V. Course of the AFM-based SMFS Measurement

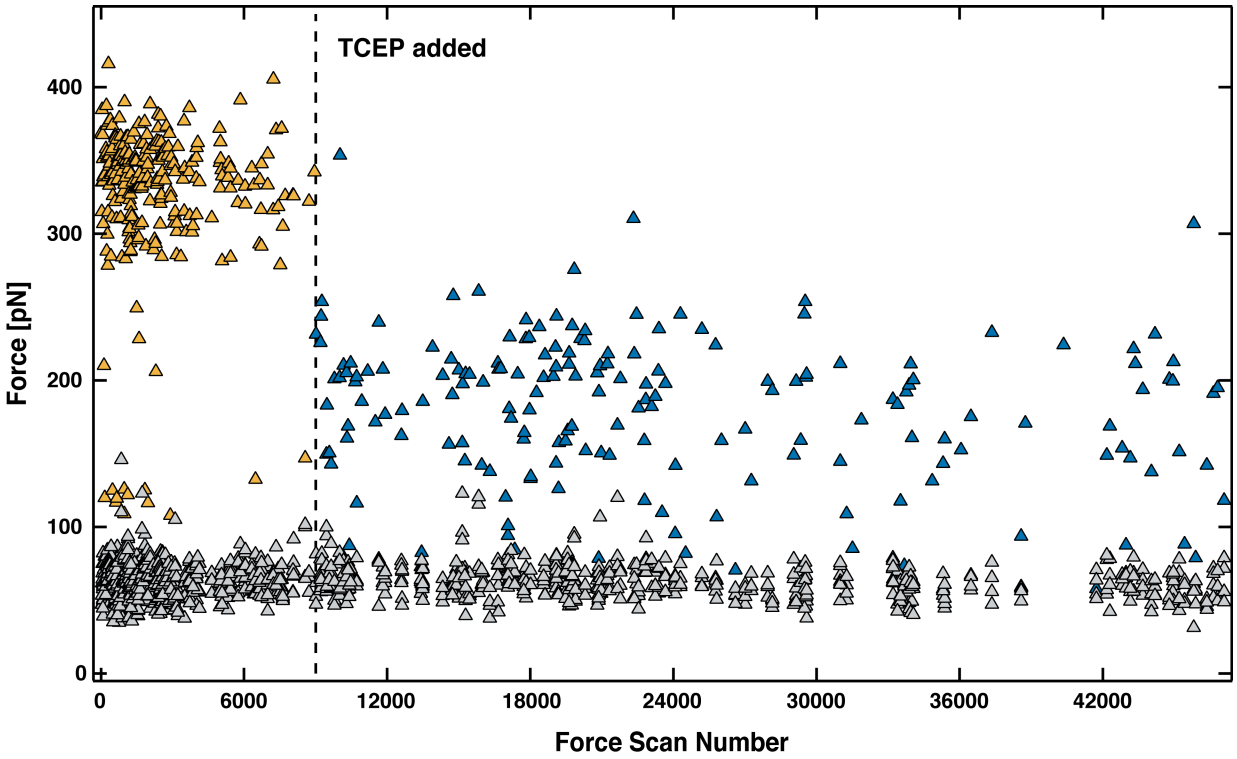

Supplementary Figure S4. Course of the AFM-based SMFS measurement for 200 nm/s retraction velocity. For all force-extension traces showing two distinct ddFLN4 unfolding pattern before the unbinding of biotin from mSA, the four ddFLN4 unfolding forces (grey) and the final biotin/mSA unbinding force (colored) are plotted over time. After about 9,000 approach-retraction cycles, the reducing agent TCEP was added to the measurement buffer (indicated by the dashed line). In the absence of TCEP (yellow), the mSA/biotin unbinding forces are significantly higher than in the presence of TCEP (blue). TCEP does not affect the unfolding forces of ddFLN4.

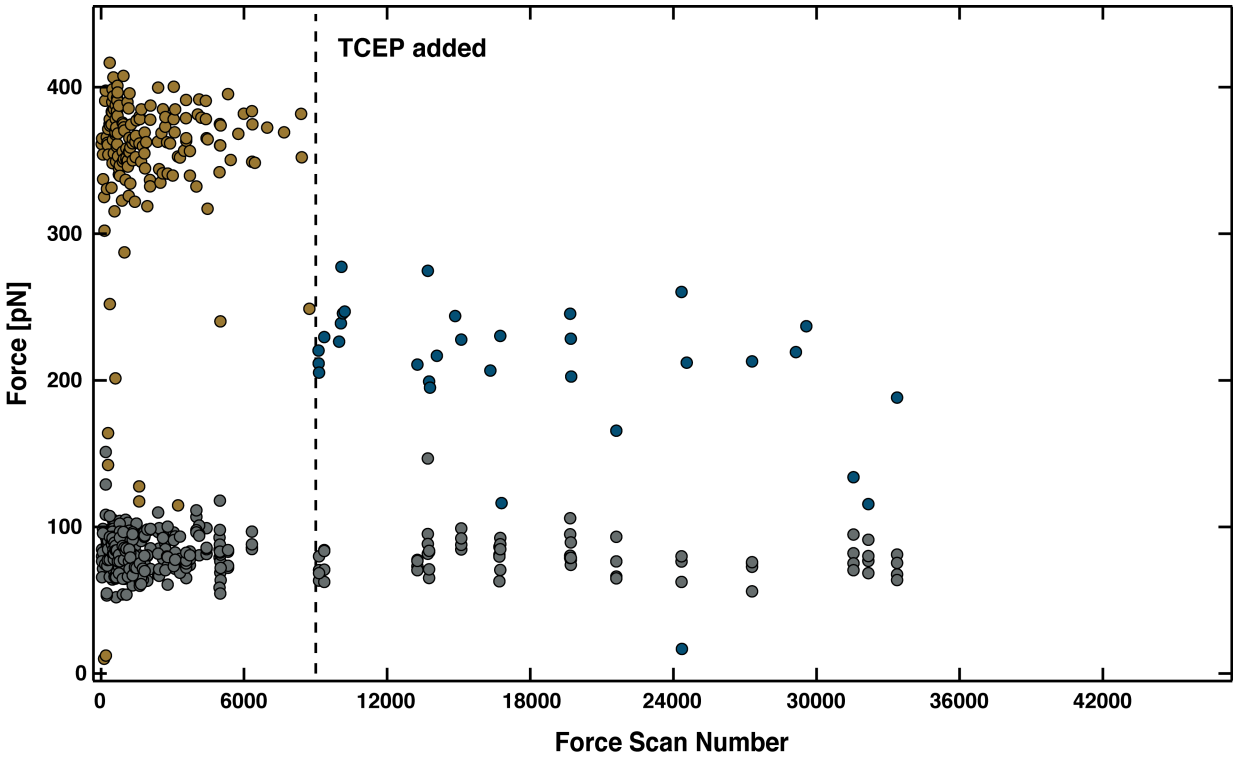

Supplementary Figure S5. Course of the AFM-based SMFS measurement for 3200 nm/s retraction velocity. For all force-extension traces showing two distinct ddFLN4 unfolding pattern before the unbinding of biotin from mSA, the four ddFLN4 unfolding forces (grey) and the final biotin/mSA unbinding force (colored) are plotted over time. After about 9,000 approach-retraction cycles, the reducing agent TCEP was added to the measurement buffer (indicated by the dashed line). In the absence of TCEP (yellow), the mSA/biotin unbinding forces are significantly higher than in the presence of TCEP (blue). TCEP does not affect the unfolding forces of ddFLN4.

VI. Inverse Experiment – TCEP from the Beginning Followed by Buffer Exchange

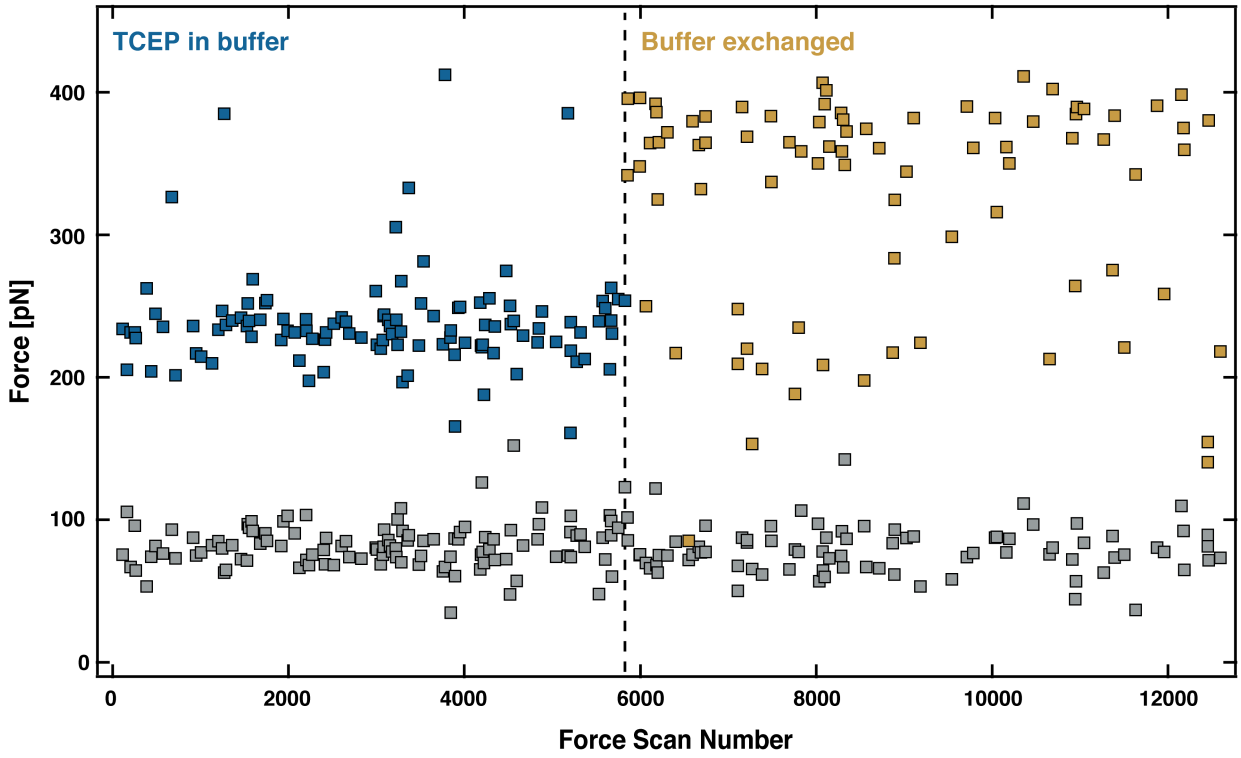

Supplementary Figure S6. Course of the inverse AFM-based SMFS measurement for 800 nm/s retraction velocity. For all force-extension traces showing two distinct ddFLN4 unfolding pattern before the unbinding of biotin from mSA, one of the four ddFLN4 unfolding forces (grey) and the final biotin/mSA unbinding force (colored) are plotted over time. The mSA construct was incubated with TCEP before surface attachment and TCEP was present in the measurement buffer from the beginning. After 5,825 approach-retraction cycles (indicated by the dashed vertical line), the surface was rinsed with 75 mL PBS buffer which had been exposed to oxygen gas in a drechsel gas washing bottle. The mSA/biotin unbinding forces after buffer exchange (yellow) are significantly higher than in the presence of TCEP (blue). Single events at lower forces, which might arise from not recovered disulfide bridges, are also observed. For this measurement, the spring constant of the AFM cantilever was 105 pN/nm.

VII. Dynamic Force Spectrum

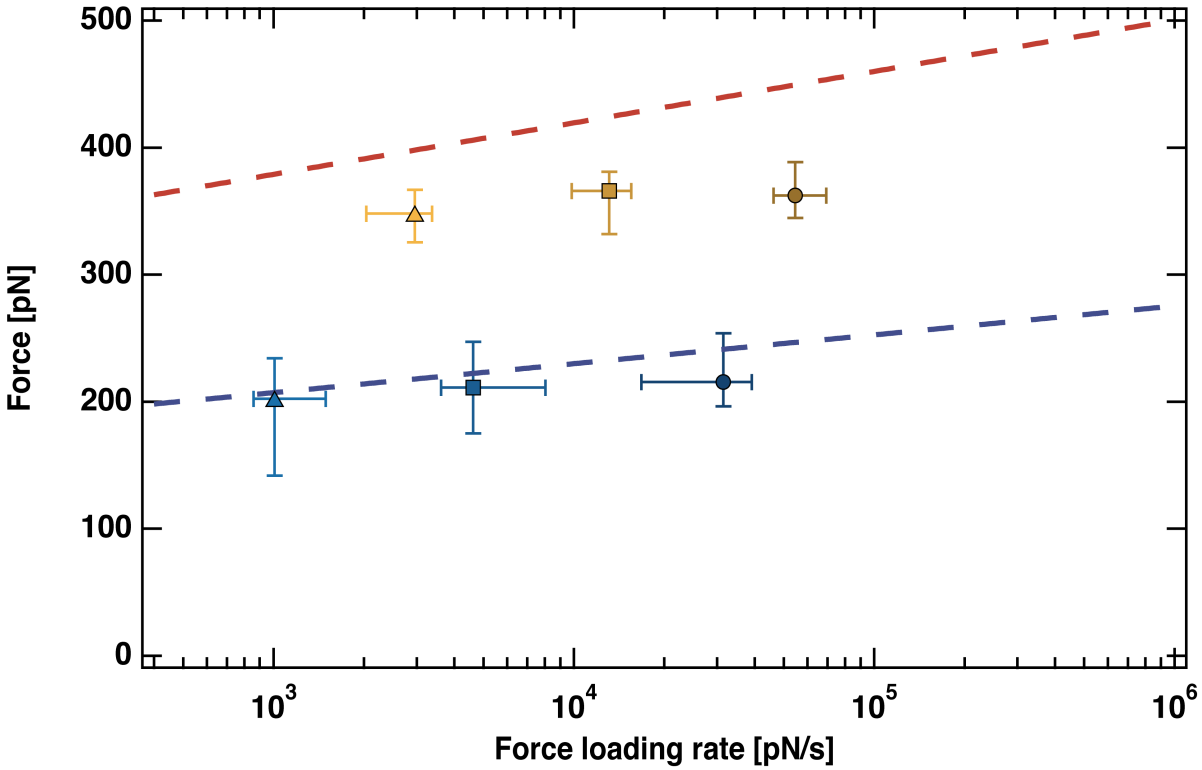

Supplementary Figure S7. Dynamic force spectrum with standard Bell-Evans fits from previous publication (Sedlak *et al.*[4]). Markers show most probable unbinding force plotted against most probable loading rate for mutated (T18C,A33C) mSA for experimental data shown in Fig. 4. Different retraction velocities used are indicated by color shade and symbol (200 nm s^{-1}: triangle, 800 nm s^{-1}: rectangle, 3200 nm s^{-1}: circle). Errors show the full width at half maximum of a kernel density estimation. Lines are fits to dynamic force spectrum of N-terminally (x_0=0.41 nm, $k_{off,0}$=7.7 x 10^{-8} s^{-1}, blue dashed line) and C-terminally (x_0=0.23 nm, $k_{off,0}$=2.5 x 10^{-8} s^{-1}, red dashed line) attached mSA, both without the mutation.[4] In the presence of TCEP (blue markers) the fit line for N-terminal attached mSA lays within the errors. In the absence of TCEP the data points (yellow markers) lay in between the two lines. Here, we don't expect an overlay with the fit line for C-terminal attached mSA, since although bearing a reinforced N-terminus the pulling geometry stills differs.

VIII. Fitting of the Bell-Evans Model

Israilev *et al.* and Evans and Ritchie independently proposed a model to characterize how an external force affects the dissociation of molecular bonds.[2, 3] The model assumes a constant force loading rate *r*, which is not true for AFM-based constant velocity force spectroscopy experiment. It is still commonly applied for AFM-based SMFS experiments. According to the model, the probability distribution of rupture forces is given by:

Physical parameters are derived from the fitting parameters *a* and *b*:

Details can be found in Sedlak *et al.*[4].

Supplementary Table S1. Fitting parameters for Figure 4.

	v_R [nm/s]	a [$\times 10^3$]	b [$\times 10^{10}$]
-TCEP	**200**	12.3	4.33
	800	20.1	4.00
	3200	9.9	4.77
+TCEP	**200**	2.0e5	2.43
	800	7.4e4	2.78
	3200	2.7e3	4.22

Supplementary Table S2. Physical parameters extracted from the data in Figure 4.

	v_R [nm/s]	<F> [pN]	<r> [pN/s]	x_0 [nm]	$k_{off,0}$ [s^{-1}]
-TCEP	**200**	350	2,700	0.18	3.3e-5
	800	360	12,400	0.17	2.5e-4
	3200	370	57,300	0.20	5.7e-5
+TCEP	**200**	200	1,100	0.10	2.3e-1
	800	210	5,300	0.12	4.0e-1
	3200	220	27,600	0.18	7.5e-2

IX. Unfolding Force Histograms for the Fingerprint Domains

Supplementary Figures S8, S9 show force histograms for ddFLN4 unfolding peaks of curves for which our software automatically identified four successive ddFLN4 unfolding peaks. In Figure 4 additional curves were taken into account featuring two ddFLN4 unfolding patterns which could not be automatically classified by the software.

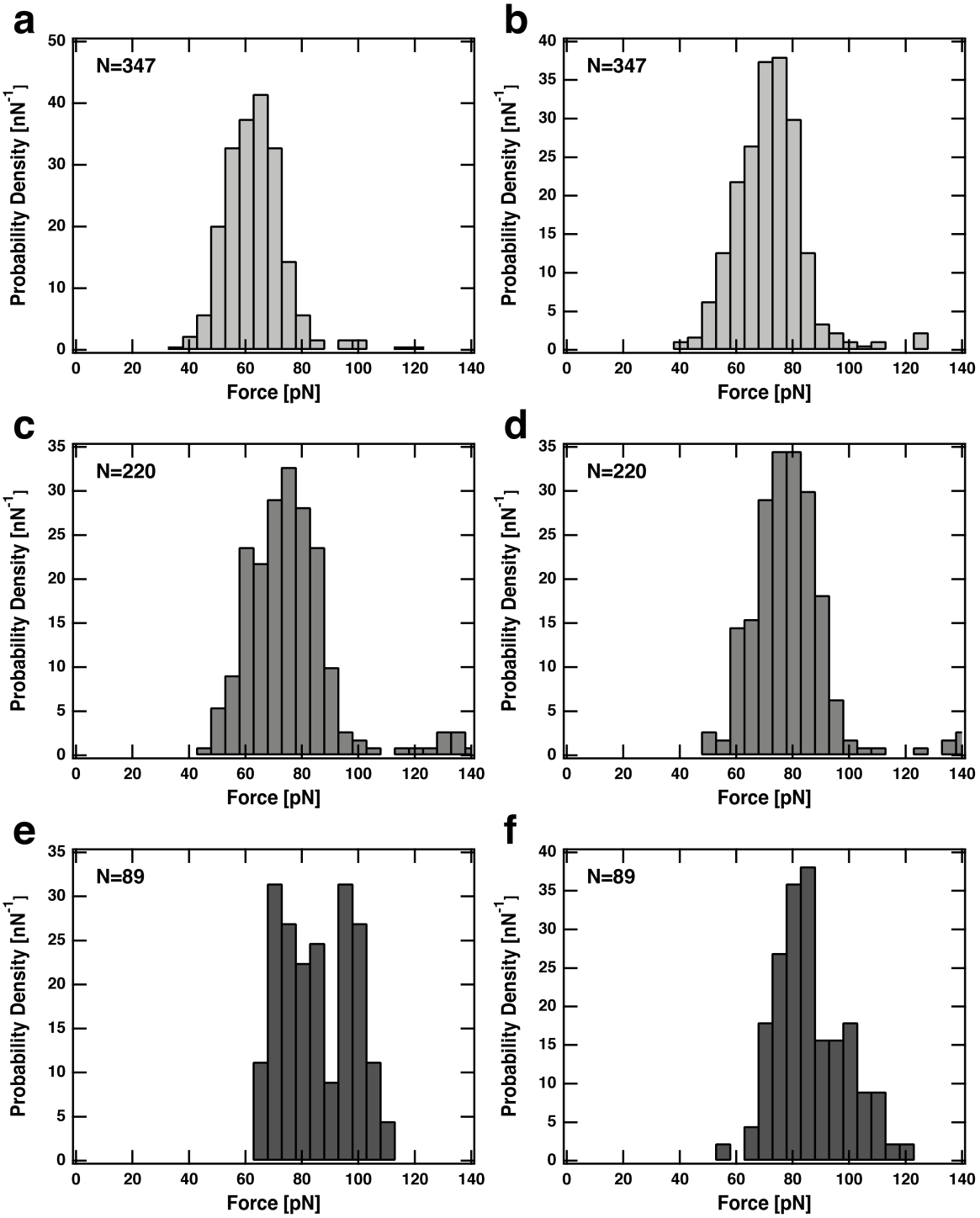

Supplementary Figure S8. Force histograms for ddFLN4 fingerprint domain fourth and third unfolding peak. (a) at 200 nm/s, (c) at 800 nm/s, (e) at 3200 nm/s show the fourth unfolding peak. (b) at 200 nm/s, (d) at 800 nm/s, (f) at 3200 nm/s show the third unfolding peak.

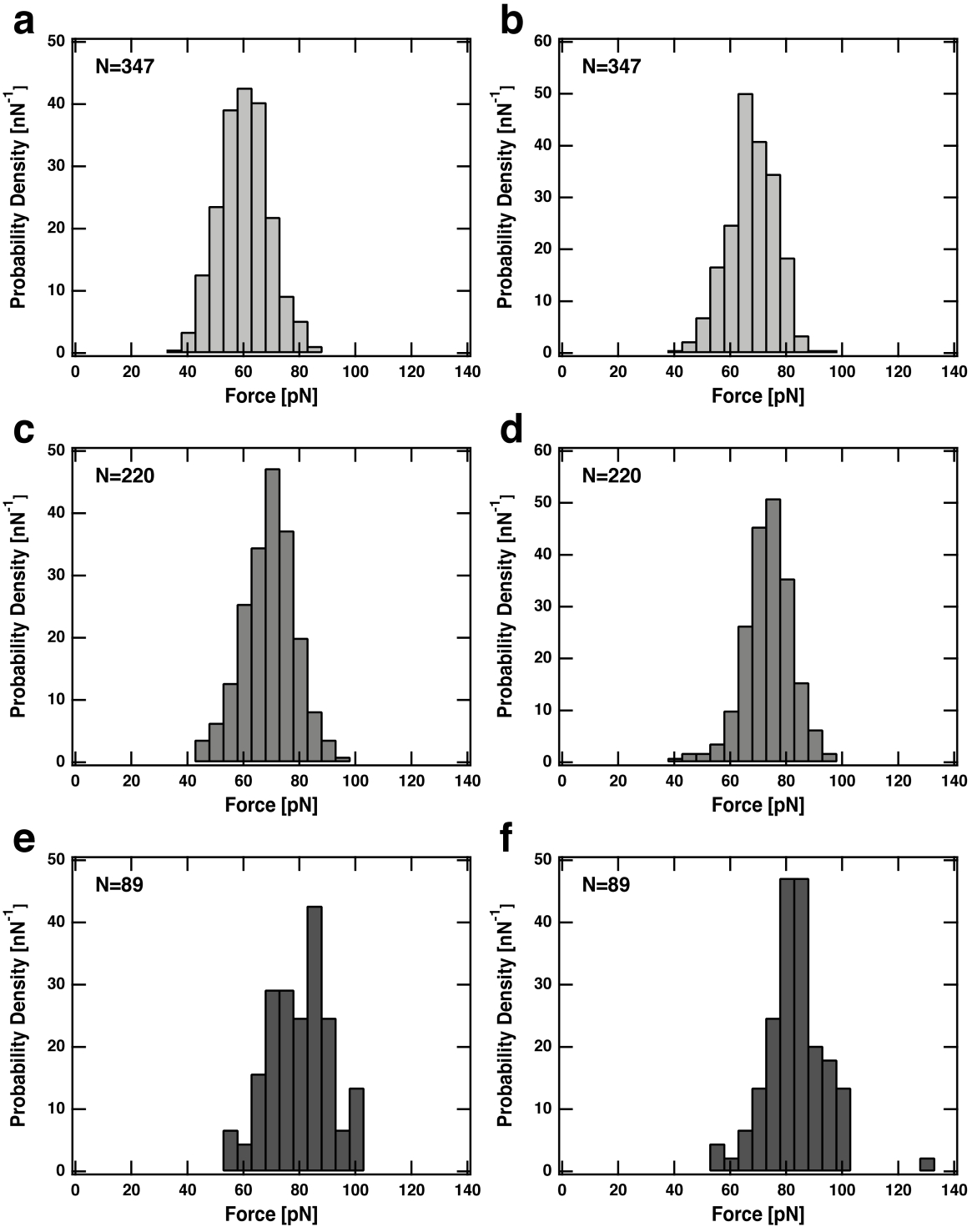

Supplementary Figure S9. Force histograms for ddFLN4 fingerprint domain second and first unfolding peak. (a) at 200 nm/s, (c) at 800 nm/s, (e) at 3200 nm/s show the second unfolding peak. (b) at 200 nm/s, (d) at 800 nm/s, (f) at 3200 nm/s show the first unfolding peak.

X. Supplementary References

1 M. Howarth, D. J. Chinnapen, K. Gerrow, P. C. Dorrestein, M. R. Grandy, N. L. Kelleher, A. El-Husseini and A. Y. Ting, *Nat Methods*, 2006, **3**, 267-273.

2 E. Evans and K. Ritchie, *Biophys J*, 1997, **72**, 1541-1555.

3 S. Izrailev, S. Stepaniants, M. Balsera, Y. Oono and K. Schulten, *Biophys J*, 1997, **72**, 1568-1581.

4 S. M. Sedlak, L. C. Schendel, M. C. R. Melo, D. A. Pippig, Z. Luthey-Schulten, H. E. Gaub and R. C. Bernardi, *Nano Letters*, 2019, **19**, 3415-3421.